DOI: 10.37190/ABB-02431-2024-03

Hemodynamic analysis of left ventricular unloading with Impella versus IABP during VA-ECMO

Honglong Yu[1,2], Yuehu Wu[2], Xuefeng Feng[2], Yuan He[2], Qilian Xie[2], Hu Peng[1*]

[1]Department of Biomedical Engineering, Hefei University of Technology, Hefei, People's Republic of China.
[2]Anhui Tongling Bionic Technology Co. Ltd, No. 5089, Wangjiang West Road, Hefei, People's Republic of China
[*]Corresponding author: Hu Peng, Department of Biomedical Engineering, Hefei University of Technology, Hefei, People's Republic of China. e-mail address: hpeng@hfut.edu.cn;

Submitted: 3rd April 2024

Accepted: 20th June 2024

Abstract

Purpose: The utilization of intra-aortic balloon pump (IABP) and Impella has been suggested as means of left ventricular unloading in veno-arterial extracorporeal membrane oxygenation (VA-ECMO) patients. This study aims to assess the local hemodynamic alterations in VA-ECMO patients through simulation analyses.

Methods: In this study, a 0D-3D multiscale model was developed, wherein resistance conditions were employed to define the flow-pressure relationship. An idealized model was employed for the aorta, and simulations were conducted to contrast the hemodynamics supported by two configurations: VA-ECMO combined with IABP, and VA-ECMO combined with Impella.

Results: Relative to VA-ECMO alone, the combination treatment had the following differences:(1) Overall mean mass flow rate increased significantly when combined with Impella and did not change significantly when combined with IABP. Blood flow pulsatility was the strongest in ECMO+IABP, and blood flow pulsatility was significantly suppressed in ECMO+Impella. (2) For all arterial inlets, HI was decreased with ECMO+Impella and increased with ECMO+IABP. (3) The flow field did not change much with ECMO+IABP, with better blood flow compliance, whereas the flow field was relatively more chaotic and disorganized with ECMO+Impella. (4) The difference between shear stress values in ECMO+IABP and ECMO alone was small, and ECMO+Impella (P6) had the largest shear stress values.

Conclusions: Variances in hemodynamic efficacy between VA-ECMO combined with IABP and VA-ECMO combined with Impella may underlie divergent prognoses and complications. The approach to ventricular unloading during ECMO and the degree of support should be meticulously tailored to individual patient conditions, as they represent pivotal factors influencing vascular complications.

Keywords: Left ventricular unloading, extracorporeal membrane oxygenation, Impella, IABP, Multiscale simulations, Hemodynamics.

Introduction

Veno-arterial extracorporeal membrane oxygenation (VA-ECMO) is primarily employed for short-term support in individuals experiencing acute, refractory cardiogenic shock [12]. Peripheral VA-ECMO facilitates blood perfusion to vital organs through retrograde blood flow; however, this mode of support augments left ventricular afterload, potentially leading to left ventricular dilatation, pulmonary edema, and thrombosis [21, 30]. Early intervention for left ventricular dilatation is advised in patients undergoing peripheral VA-ECMO support to mitigate complications arising from increased left ventricular afterload [3]. Various strategies, including atrial septostomy, LV venting, intra-aortic balloon pump (IABP), and Impella, have been proposed for left ventricular unloading [3, 11]. Among these, IABP and Impella represent the least invasive and readily available options for left ventricular unloading [13]. Nevertheless, consensus regarding the optimal left ventricular unloading strategy for VA-ECMO patients remains elusive. Furthermore, clinical data on the hemodynamic alterations induced by left ventricular unloading using IABP or Impella devices in VA-ECMO patients are scarce [9, 21, 30]. Thus, there is a compelling need to conduct numerical analyses to evaluate the hemodynamic status resulting from left ventricular unloading with IABP or Impella devices in VA-ECMO patients.

The conventional approach of employing a lumped parameter (LP) model lacks the capacity to provide quantitative analysis of the hydrodynamic state within the aorta [34]. Computational Fluid Dynamics (CFD) represents a discipline that integrates fluid dynamics theory with advancements in computer technology. CFD employs numerical computation methods to solve governing equations describing fluid motion, enabling the study of various complex phenomena related to fluid motion. It allows for qualitative and quantitative analysis of hemodynamic blood flow states non-invasively [6]. However, it's essential to carefully define boundary conditions, as they significantly influence the solution obtained through CFD. To address these limitations, a multiscale model has been developed, combining LP and CFD approaches. This model enables the study of physiological blood flow during both rest and exercise, as well as facilitating hemodynamic analysis of ventricular assist device outflow

grafting positions [19, 24]. By incorporating dynamic boundary conditions using a three-element lumped parameter model, this model simulates the impact of various devices on hemodynamics. Yet, there currently exists no multiscale simulation method capable of comparatively analyzing hemodynamics under different ventricular unloading strategies.

The objective of this study was to delineate the specific local hemodynamic impacts associated with the use of IABP and Impella for ventricular unloading in VA-ECMO patients. To achieve this, we constructed a multiscale coupled model encompassing the cardiovascular system and the aorta. This model facilitated an evaluation of the effects resulting from the utilization of the two mechanical circulatory support (MCS) combinations on the aorta. The primary hemodynamic indices considered in this assessment comprised the flow pattern, blood flow harmonic index (HI), blood flow distribution, and wall shear stress (WSS).

Materials and Methods

Geometrical Modelling

In order to study the hemodynamic situation of the aortic system, the 3D software SolidWorks 2016(Dassault Systemes Simulia Inc., France) was used to build an ideal 3D structural model of the aorta, which contains the main aortic outlets, including the brachiocephalic artery(BCA), left common carotid artery(LCCA), left subclavian artery(LSA), superior mesenteric artery(SMA), celiac artery(CA), inferior mesenteric artery(IMA), left common Iliac(LCI), right common iliac(RCI), left renal artery(LRA), right renal artery(RRA)[2, 28, 35].

With reference to the VA-ECMO connection, a 24 Fr arterial cannula (Medtronic Inc., Minneapolis, MN, USA) was reconstructed and placed in the iliac aorta (Figure 1).

A 40cc IABP (Sensation 7 Fr 40 cm^3 and CS300 IABP System, Datascope, Maquet GmbH and Co. KG, Rastatt, Germany) balloon and an Impella CP (14Fr, Abiomed, America) pump were modeled using the software SolidWorks 2016, as shown in Figure 1. It is worth noting that we drew on relevant literature to build the specific model of Impella CP[29]. The three-dimensional structural model of the Impella CP was divided into an impeller section and an extension section, where the impeller section mainly consists of the pump casing, the rotor

shaft and the vanes of the spiral. In order to ensure that the fluid flow in the tube has full development, the extension section is 5 times longer than the tube diameter of the impeller section. The two ends of the pump shell are inflow and outflow ports, with the inflow port in the left ventricular outflow tract and the outflow port in the aorta. The cross-sectional grid structure of the Impella CP, as well as the location of the Impella CP and its partially enlarged details are shown in Figure 1(A).

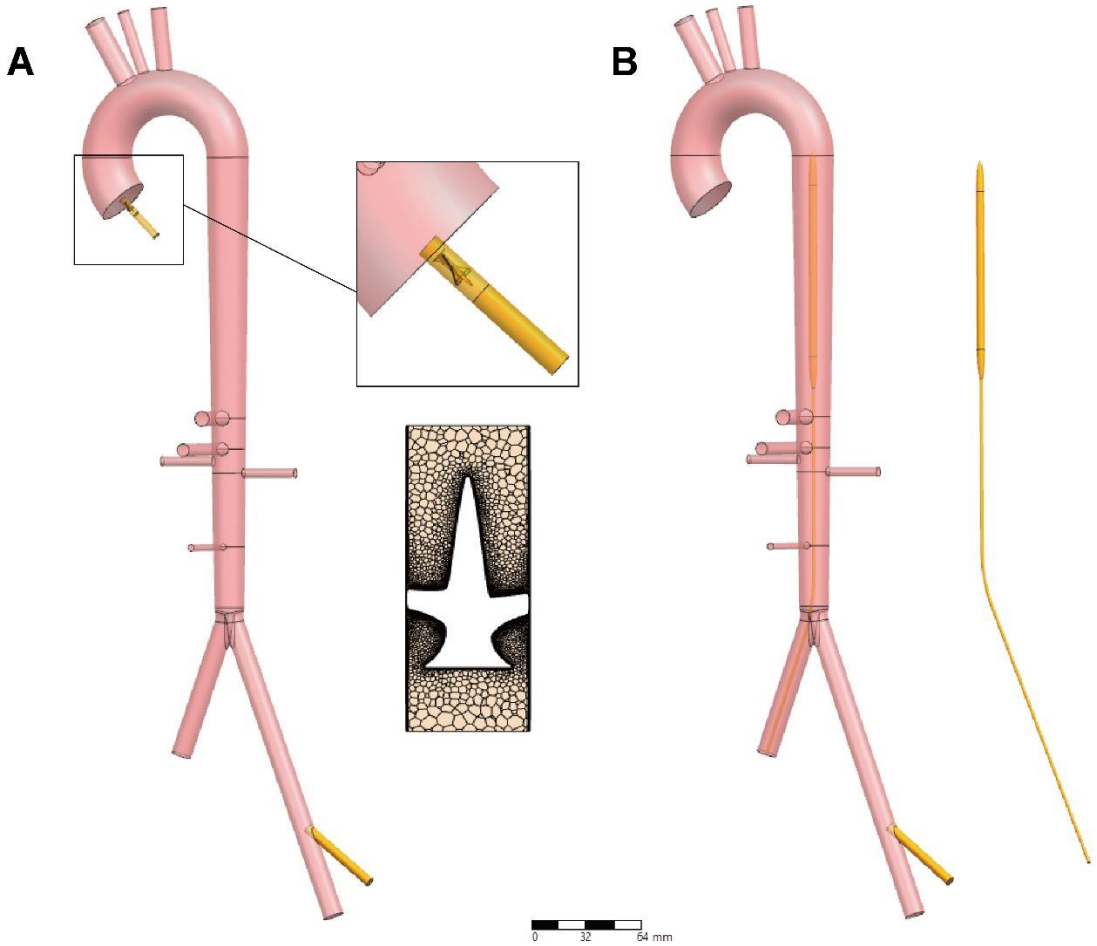

Figure 1. 3D geometric model of Impella(A) and IABP(B).

Mathematical Models

For a large vessel like the aorta, blood can be modelled as an incompressible Newtonian fluid with a viscosity of 0.0035 Pa·s. and a density of 1060 Kg/m^3. *In vivo*, blood is a non-Newtonian fluid with complex shear-thinning behavior, which cannot be ignored in smaller vessels like coronary arteries. But in large vessels like aorta, with shear rates up to >300 s^{-1}, modeling blood as a Newtonian fluid can serve as a reasonable approximation while

maintaining accuracy and improving efficiency[4, 25, 27]. Furthermore, the motion of the blood flow was described by the three-dimensional Navier-Stokes equations:

$$\nabla \cdot u = 0 \quad (1)$$

$$\rho(\partial u/\partial t) + \rho(u \cdot \nabla)u = \nabla \cdot [-pI + \mu(\nabla u) + (\nabla u)^T] + F \quad (2)$$

Where *u, p, μ, ρ, I* and *F* represent the fluid velocity vector, pressure, dynamic viscosity, blood density, unit matrix, and volumetric force field respectively. The finite volume method was used to describe the fluid motion for solving the Navier-Stokes equations.

The three-dimensional shear stress scalar used in this paper was extracted from the velocity flow field of numerical simulation. the scalar stress was calculated as follows:

$$\tau_{ij} = \sigma_{ij} + \rho\overline{u_i' u_j'} \quad (3)$$

$$\sigma_{ij} = \mu\left(\frac{\partial u_i}{\partial x_j} + \frac{\partial u_j}{\partial x_i}\right) \quad (4)$$

$$\tau = \left[\frac{1}{6}\sum(\tau_{ii} - \tau_{jj})^2 + \sum \tau_{ij}^2\right]^{\frac{1}{2}} \quad (5)$$

The turbulent shear τ_{ij} was formed by combining the viscous shear σ_{ij} with the Reynolds shear stress $\rho\overline{u_i' u_j'}$, where *i,j*=1,2,3 represent the x,y,z directions, respectively; μ stands for the dynamical viscosity; and u_i, u_j stand for the mean velocity components in each direction.

The inflation and deflation process of the IABP balloon synchronized with the cardiac cycle, and its inflation/deflation behavior was numerically reproduced in the simulation by changing the balloon radius parameter[17], whose radius varied during the cardiac cycle as shown in Figure 2.

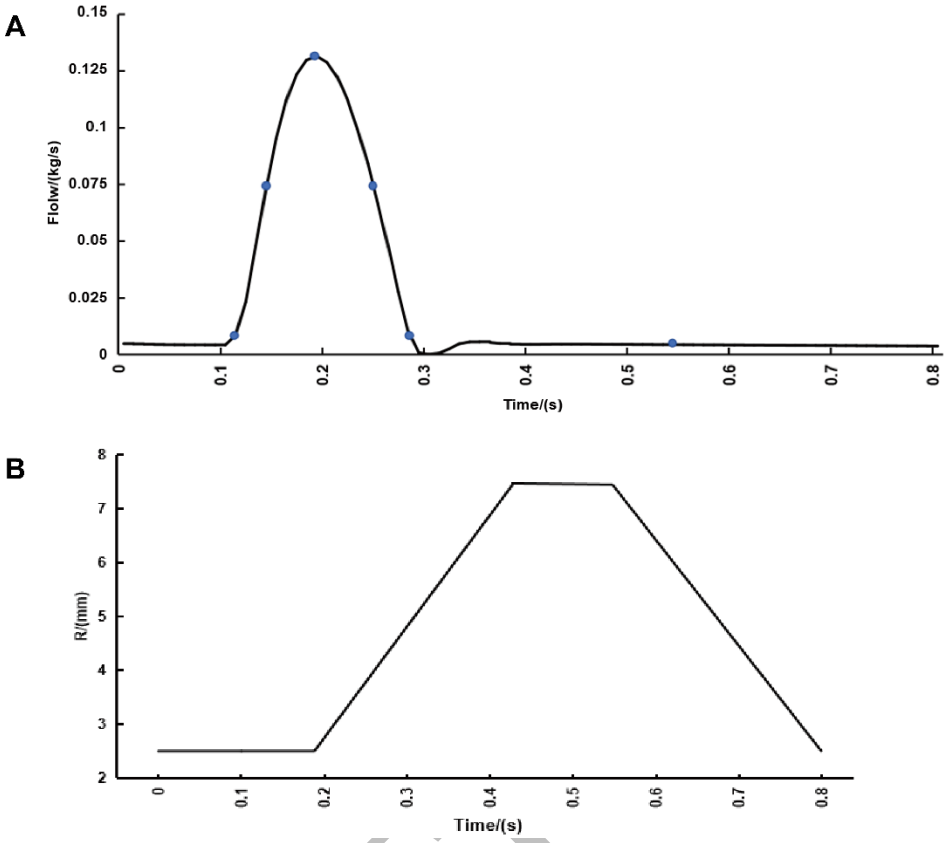

Figure 2. Behavior of ventricular flow changes(A) and IABP radius changes(B) during one cardiac cycle.

Note: Peak systolic IABP off, mid diastolic IABP on.

The different speeds of the Impella CP correspond to different flow rates, which were used as inlet boundary conditions. The flow rate of Impella CP was obtained based on the pressure and flow characteristics. Impella CP was modeled using second order polynomial equations and the pressure-flow characteristics were obtained from the instruction manual.

Boundary conditions and Grid independence verification

To compare the hemodynamic effects of Impella and IABP on the aorta when combined with VA-ECMO, respectively, the following four simulations were performed:

1. ECMO implantation (2000 r/min).

2. Fixed ECMO speed (2000r/min) and Impella contribution at P2(Low flow rates).

3. Fixed ECMO speed (2000r/min) and Impella contribution at P6(High flow rates).

4. Fixed ECMO speed (2000r/min) and IABP support（Counterpulsation ratio 1:1）

The four combinations were all based on ANSYS Fluent using a combination of mass flow inlet and pressure outlet for transient simulation, the number of boundary layers was 10, the turbulence model was selected as SST k-ω model, the turbulence intensity was set to 5%, the wall surfaces were all set to be no-slip wall surfaces, and the convergence criterion was set to 0.0001. Impella at P2 and P6 with impeller speeds of 31,000 and 39,000 rpm and flow rates of 1.5 and 2.7 L/min, respectively. The IABP balloon inflation and deflation process was realized by means of UDF calling the DEFINE_GRID_MOTION macro. This simulation took 0.8 seconds as a cardiac cycle, and a total of 2.4 seconds of hemodynamic states were calculated, and all the simulation data in this paper were based on the simulation results of the last cardiac cycle.

In this study, five different grid numbers were used to verify the independence of the grids, which were 917021, 1037235, 1147956, 1297274 and 1439006, respectively. By monitoring and counting the inlet and outlet mass flow, the independence of the grids was tested by comprehensively comparing the size of the gap between the two under different grid numbers.

After comparison, it was found that when the number of grids was greater than 1297274, the inlet and outlet flow rate error was less than 1%, the average shear value was almost unchanged, the influence of the number of grids on the calculation results was negligible, as shown in Figure 3. Therefore, in order to minimize the computational cost under the condition of ensuring the simulation accuracy, the number of model grids used in this simulation was finally determined to be 1297274. The grid quality distribution is shown in the table below:

Table 1. Grid quality distribution.

Grid quality	<0.62	0.62~0.72	0.72~0.81	0.81~0.91	0.91~1
Percentage of grids (%)	1.598	13.576	11.596	12.137	61.093

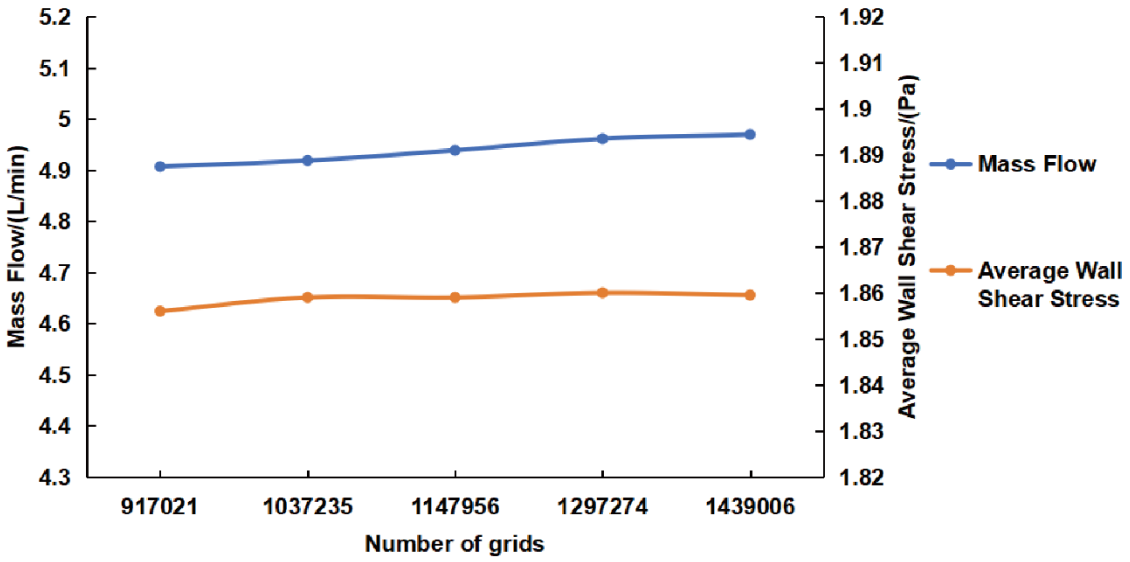

Figure 3. Mesh independent verification results.

To study hemodynamic effects, the pulsatile flow rate (mean 1 L/min), derived from the validated lumped-parameter (LP) model, served as the inlet boundary condition[14, 16, 18].

The aortic outlets used dynamic boundary conditions to determine the effect of changing blood flow patterns on perfusion and were modeled using a three-element lumped parameter model of distal vascular impedance[25] (Figure 4B). This zero-dimensional electrical analogy of the hemodynamic system ensured that the characteristics of each aortic outlet and distal resistance and vascular compliance were considered. The relationship between flow and pressure in each branch was described by the following differential equation:

$$\frac{\partial_P}{\partial_t} + \frac{p}{CR_d} = \frac{Q}{c}\left(1 + \frac{R_P}{R_d}\right) + R_P\frac{\partial Q}{\partial t} \quad (6)$$

Where Q, p, R and C represent the inflow to the lumped element, the inlet pressure, the resistance (subscript p and d stand for the proximal and distal component), and the compliance of the lumped element. Computational analysis was performed on a local parallel processing cluster. Hemodynamic characteristics, stress indicators, and end-organ perfusion were measured for each simulation. Table 2 shows the parameters of each artery. At each time step, each exit branch was solved and updated.

Table 2. Parameters of Three-Element Lumped Parameter Model for Aorta[25].

Artery	R_P (10^7Pa·s·m^{-3})	R_d (10^8Pa·s·m^{-3})	C(10^{-10}·m^3·Pa^{-1})
BCA	5.192	10.608	8.697
CA	11.762	7.573	12.184
IMA	74.017	46.225	1.996
LCCA	19.152	52.213	1.767
LCI	5.915	10.174	9.069
LRA	34.138	5.395	17.102
LSA	9.882	13.018	7.087
RCI	5.915	10.174	9.069
RRA	34.138	5.395	17.102
SMA	17.435	5.510	16.745

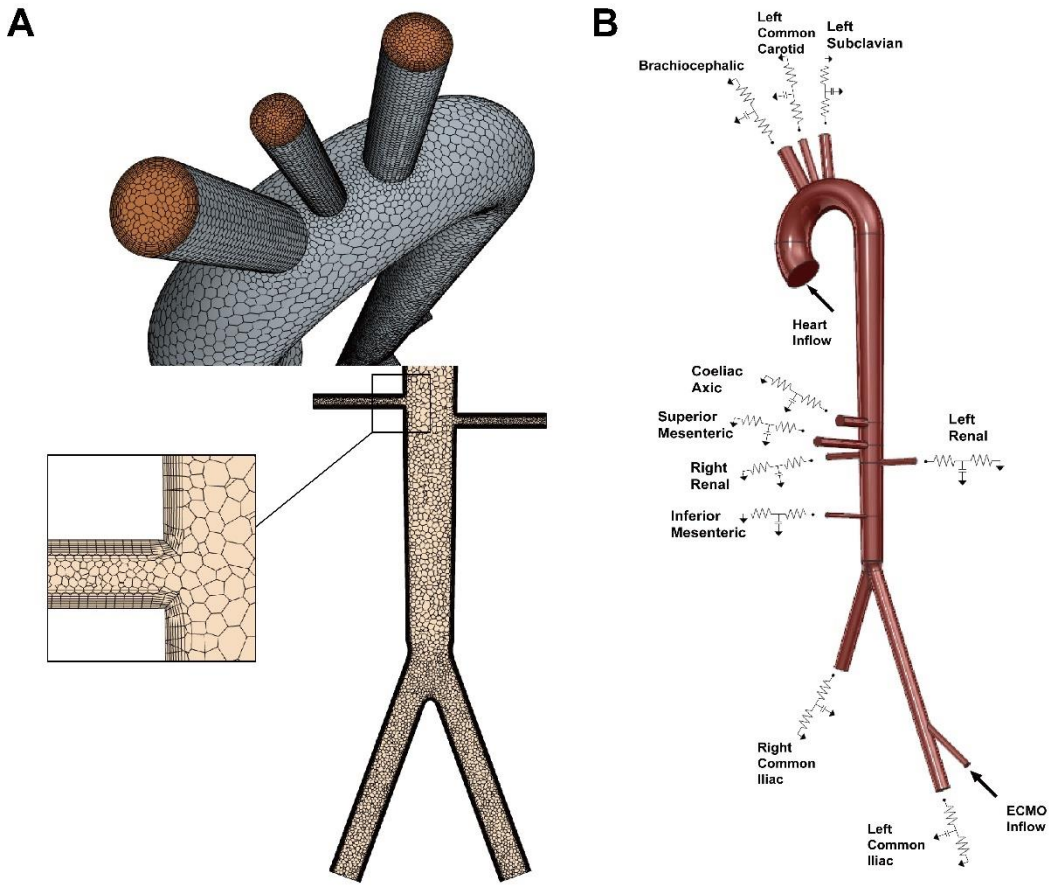

Figure 4. A: Polyhedral volumetric grids with different views and cross-sections. B: Coupling the three-element lumped parameter dynamic boundary conditions to an ideal three-dimensional computational null-center model.

To assess the pulsatility of the flow, the Harmonic Index (HI) was used. The Harmonic Index was a measure of the relative contribution of the non-stationary intensity to the overall signal strength, ranging from 0 (a steady, non-zero flow signal) to 1 (a pure oscillating signal with zero averaging time). HI was defined as equation (7):

$$HI = \frac{\sum_{n=1}^{+\infty} T[nw_0]}{\sum_{n=0}^{+\infty} T[nw_0]} \quad (7)$$

Among them, $T[nw_0]$ denotes the size of the converted flow rate signal.

Results

Computational analysis of VA-ECMO combined with IABP or Impella was performed using an aortic model. WSS, velocity, flow, and HI were simulated at different combinations of relative VA-ECMO flow to test different hemodynamic profiles.

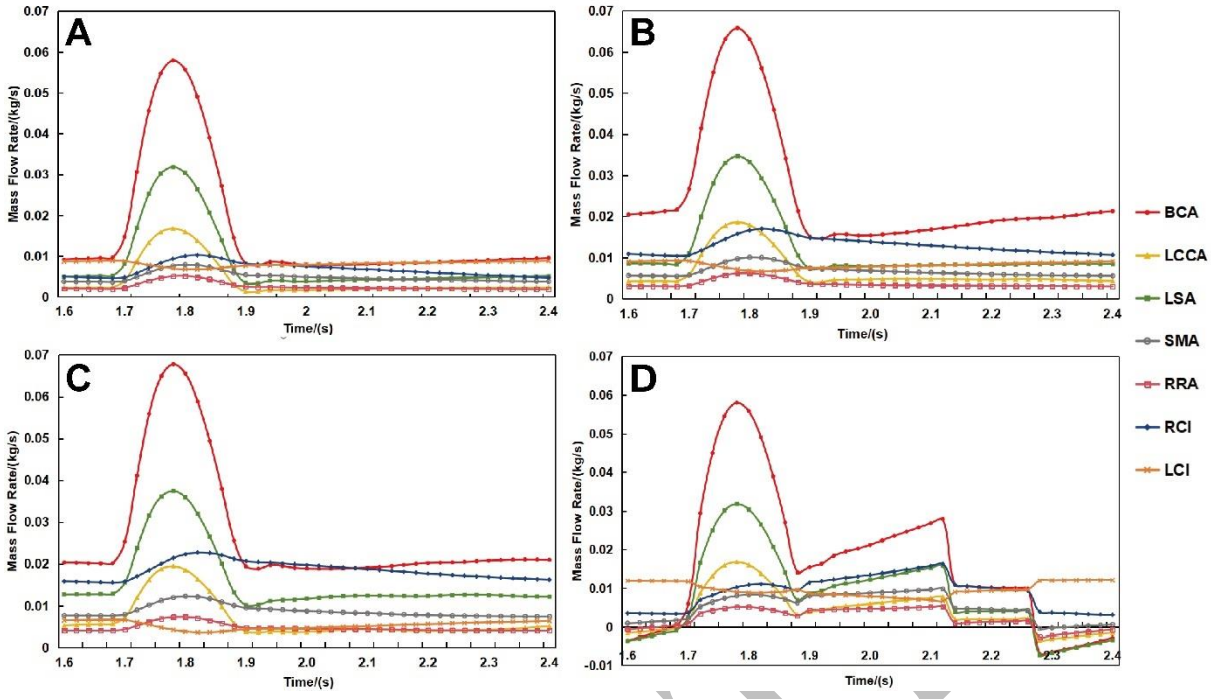

Figure 5. Mass flow rate profiles of the main arterial outlets during one cardiac cycle under four different circulatory assist support conditions. (A) is the flow rate during ECMO alone, (B) is the flow rate during ECMO+Impella(P2). (C) is the flow rate at ECMO+Impella (P6). (D) is the flow rate at ECMO+IABP.

Figure 5 shows mass flow rate profiles of major arterial inlets during a cardiac cycle for four different circulatory assist support conditions, providing the hemodynamics of blood flow pulsation and vital organ perfusion according to their location proximal and distal to the aorta.

With ECMO alone and ECMO+Impella, mass flow peaked in systole and decreased gradually in diastole. With ECMO+IABP, mass flow peaked in systole and showed multiple flow fluctuations in diastole. BCA flow was greater than the rest of the inlet flow.

Table 3. Average flow rate at each outlet for four operating conditions.

(Unit: 10^{-3}kg/s)

	ECMO	ECMO+Impella(P2)	ECMO+Impella(P6)	ECMO+IABP
BCA	12.942	20.363	21.751	13.302

LCCA	3.402	5.326	5.326	3.426
LSA	6.881	9.721	12.689	6.656
SMA	3.908	5.376	6.948	4.205
RRA	2.066	2.88	3.772	1.862
RCI	5.389	10.314	14.804	7.26
LCI	6.487	6.505	4.216	7.739

Table 3 shows the mean mass flow at the inlet of the main arteries under four different circulatory auxiliary support conditions. ECMO+Impella significantly increased the overall mean mass flow rate compared with ECMO alone, such as at the inlet of BCA, LCCA, LSA, CA, SMA, left and right renal artery and IMA, and ECMO + Impella (P6) provided greater overall mean mass flow than ECMO+Impella (P2). The mean mass flow rate of ECMO+IABP was almost the same as that of ECMO alone.

For LCI artery inlet mean mass flow, it did not increase with ECMO+Impella relative to ECMO and was reduced with ECMO+Impella (P6), and it increased with ECMO+IABP relative to ECMO alone.

Table 4. HI of inlet flow to these major arteries under four different conditions.

	ECMO	ECMO+Impella(P2)	ECMO+Impella(P6)	ECMO+IABP
BCA	0.7271	0.6056	0.6077	0.7668
LCCA	0.734	0.6553	0.6543	0.7848
LSA	0.7372	0.659	0.5911	0.7844
SMA	0.4207	0.2723	0.3417	0.5669
RRA	0.5393	0.4194	0.3098	0.7174
RCI	0.4458	0.2597	0.2108	0.4751

LCI	0.22	0.1417	0.2324	0.2285

Table 4 shows the HI of major arterial inlet flows for the four different circulatory assist support scenarios. With ECMO+Impella, the HI of all arterial inlet flows was lower than that of ECMO, and with ECMO+IABP, the HI of all arterial inlet flows was higher than that of ECMO.

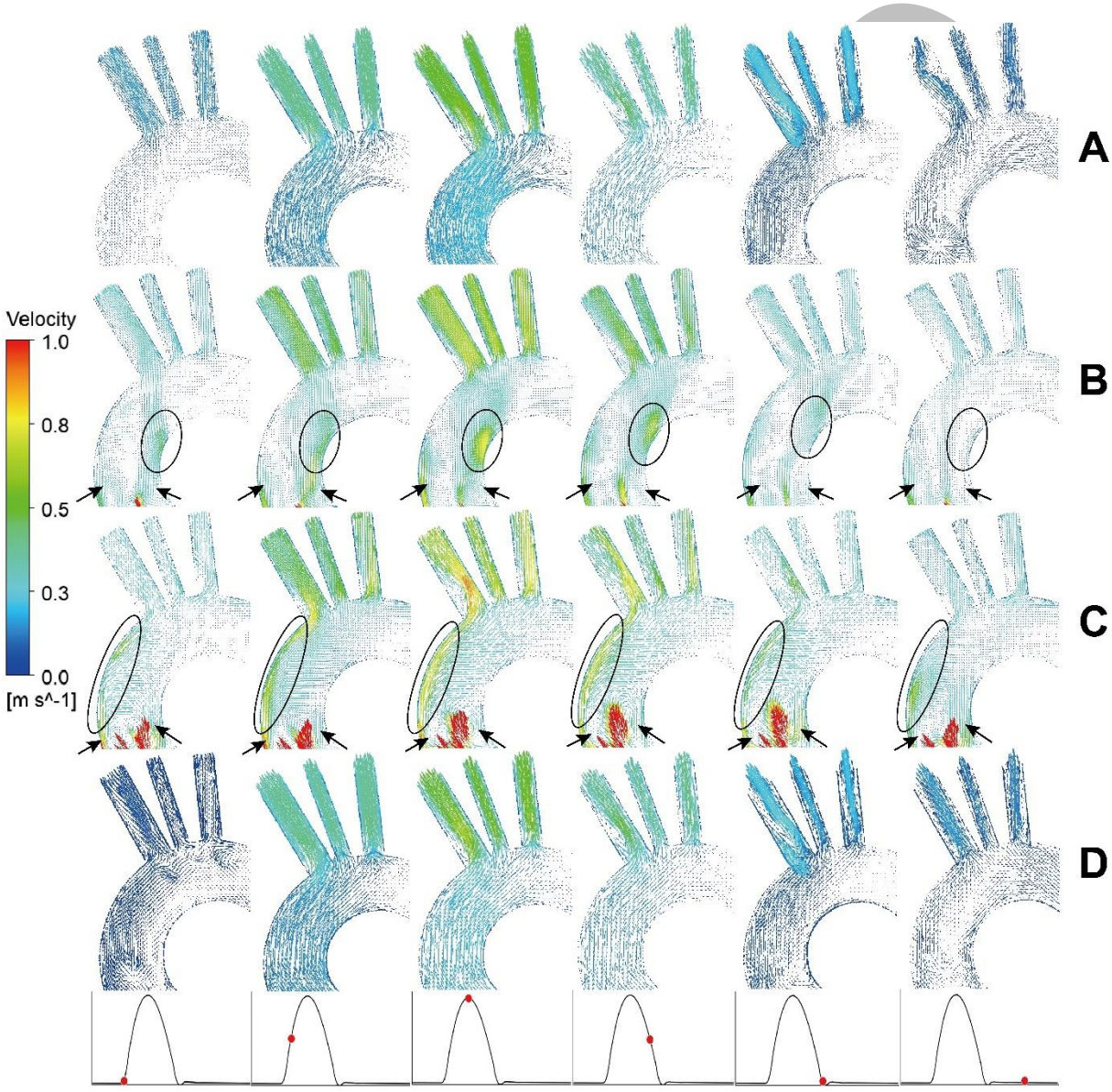

Figure 6. Velocity vectors of the aortic arch region at different moment points in a cardiac cycle under four different circulatory assist support conditions, the moment points have been labelled in Figure. 2A. (A) is the velocity vector for ECMO alone, (B) is

the velocity vector for ECMO+Impella(P2). (C) is the velocity vector for ECMO+Impella(P6). (D) is the velocity vector of ECMO+IABP.

As shown in Figure 6, the overall flow was higher during cardiac systole and gradually decreased during diastole. Flow rates were greater in the BCA, LCCA, and LSA. The flow field of ECMO+IABP did not change much relative to that of ECMO alone, and blood flow compliance was better. The flow field of ECMO+Impella was more chaotic and disorganized relative to that of ECMO alone.

Ascending aortic flow rates were more variable with ECMO+Impella, which was mainly due to the larger jet flow rate provided by Impella. In the region of the ascending aortic outlet, vortices appeared on both sides of the Impella-jetted high-velocity blood flow, as shown by the arrows in Figures 6(B) and 6(C). ECMO+Impella (P2) showed an area of high flow rate on the medial side of the ascending aorta, as shown by the circle in Figure 6(B); ECMO+Impella (P6) showed an area of high flow rate on the other side of the ascending aorta, as shown by the circle in Figure 6(C).

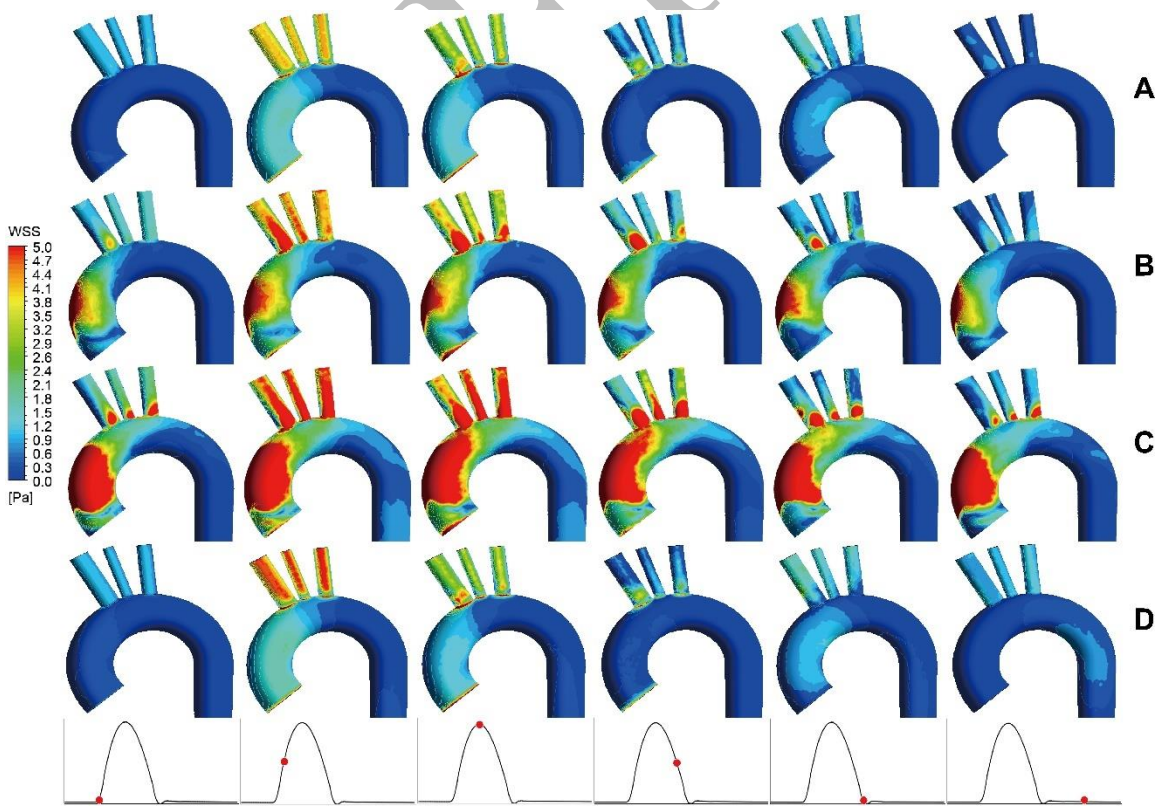

Figure 7. WSS contours of the aortic arch region at different moment points in a cardiac cycle under four different circulatory assist support conditions. (A) is the WSS

contour for ECMO alone, (B) is the WSS contour for ECMO+Impella(P2). (C) is the WSS contour for ECMO+Impella(P6). (D) is the WSS contour for ECMO+IABP.

As shown in Figure 7, the high WSS zones of the aortic arch were different in the four different circulatory assisted support conditions. The BCA, LCCA, and LSA inlets were the high WSS zones (up to 3.2 Pa) when ECMO alone was used, and the area of the posterior wall of the aortic arch that corresponded to the outlet of the Impella was the high WSS zone when ECMO+Impella was used. ECMO+Impella (P6) and ECMO+Impella (P2) corresponded to peak WSS values of 27 Pa and 15 Pa, respectively. The peak WSS values in ECMO+IABP were for the BCA, LCCA, and LSA exit locations, and peaked at 3.6 Pa during balloon systole.

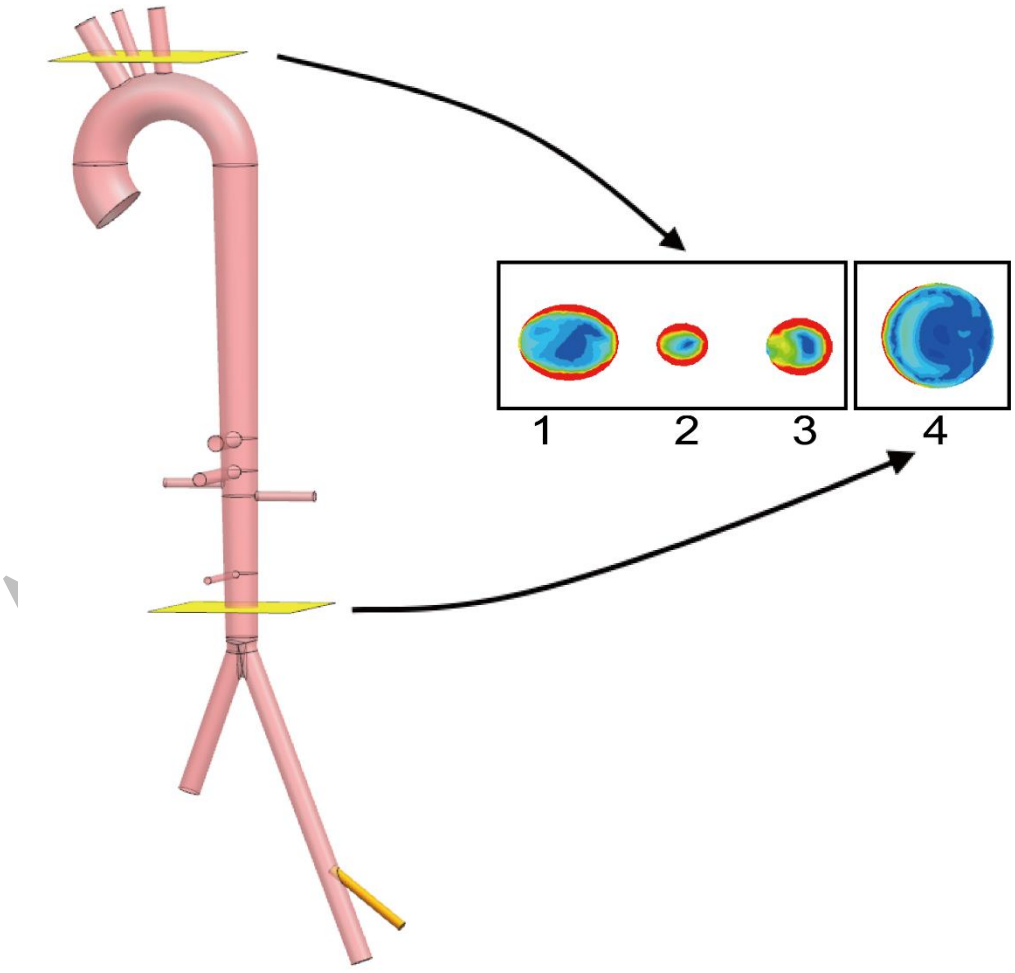

Figure 8. Schematic cross-section.

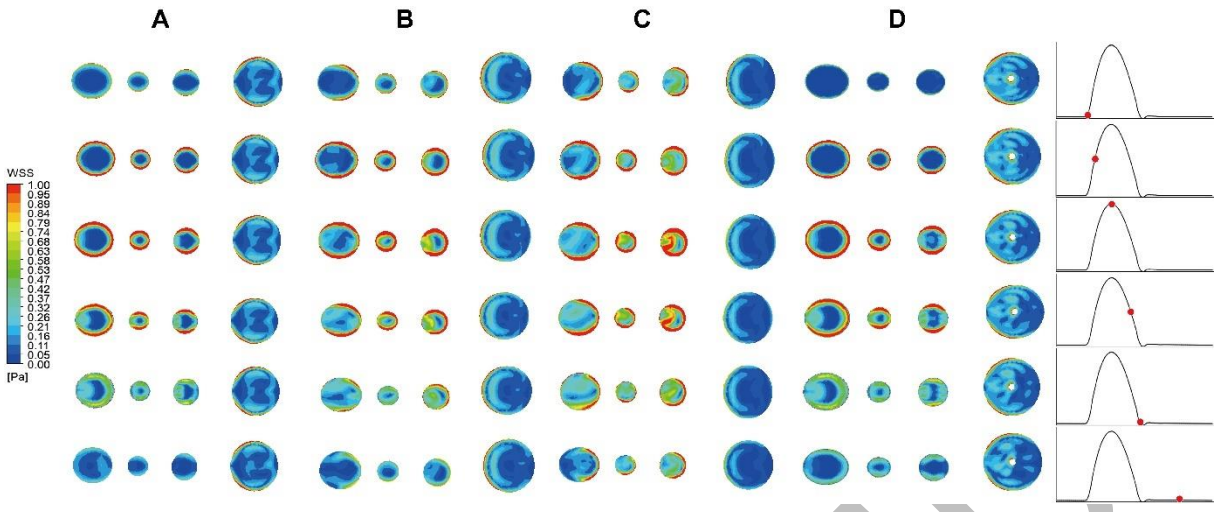

Figure 9. Cross-sectional shear stress distribution.

As shown in Figure 8, to further observe the distribution of shear stresses within the aorta, the values of shear stresses at this cross-section were obtained by inserting a plane underneath the supra-aortic vessels and the inferior mesenteric vessels. Figure 9 shows the distribution of shear stresses (WSS) in the four sections at different moment points in a cardiac cycle for four different cases of cyclic assisted support. It was observed that the shear stresses at sections 1, 2, and 3 were relatively high, whereas at section 4, the shear stress distributions of the various combinations of circulatory aids varied, but the average values were all lower. At each section, the closer to the vessel wall the higher the values of shear stresses were, whereas the shear stresses at the center of the vessel wall were relatively small. The difference between the shear stress values in ECMO+IABP and ECMO alone was small, with the largest shear stress values in ECMO+Impella (P6).

Discussion

Left ventricular unloading holds significance in the management of patients undergoing VA-ECMO, and various strategies have been employed for this purpose [5, 8, 11, 20-23, 26, 30, 32]. Clinical interventions such as combining VA-ECMO with IABP have long been utilized to enhance pulsatility, mitigate afterload, and ameliorate blood flow within coronary arteries and bypass grafts. Despite an increase in stroke volume, simulations suggest that this combined approach offers only limited left ventricular unloading. Furthermore, the

combination of IABP with ECMO does not exhibit significant associations with improved survival outcomes, prompting some studies to refrain from recommending the routine integration of VA-ECMO and IABP. Conversely, the combination of ECMO and Impella holds theoretical superiority over ECMO combined with IABP, as it offers greater circulatory support and demonstrates substantial potential for left ventricular unloading [11].

Nevertheless, numerous studies have indicated that the ECMO-Impella combination lacks statistically significant clinical benefits [3]. This observation might be attributed to hemodynamic alterations and associated complications arising from the concurrent use of both devices [15].

To date, there remains a paucity of clinical data regarding the hemodynamic alterations induced by left ventricular unloading in VA-ECMO patients utilizing IABP or Impella devices [9]. While Molfetta *et al.* [10] and Donker *et al.* [11] have simulated and compared the hemodynamic effects of various common methods of left ventricular unloading during VA-ECMO using lumped parameter models, these approaches offer limited insight into detailed local hemodynamics, such as three-dimensional blood flow patterns, organ perfusion, and wall shear stress (WSS), which can only be approximated through multiscale simulation.

To achieve this goal, a 0D-3D multiscale model was established for the first time in this study, coupling the cardiovascular lumped parameter model with the 3D model of the aorta, using resistance conditions to specify the relationship between flow and pressure. The primary aim is to compare the hemodynamic disparities between IABP and Impella during left ventricular unloading in VA-ECMO patients. Additionally, the study seeks to elucidate the hemodynamic variables and perfusion conditions influencing the utilization of these two devices in combination, with the ultimate goal of providing recommendations to mitigate the risk of hemodynamic complications.

In instances of lung disease, alterations in the contribution of ECMO support lead to distinct perfusion patterns, thereby influencing hypoxia in vital organs [33]. Both IABP and Impella, when utilized for ventricular unloading in VA-ECMO patients, elevate the flow of hypoxic blood originating from their respective hearts, comprising the physiological ejection

of the heart and the supplementary blood flow from Impella. Inadequate oxygenation delivered to critical organs such as the coronary arteries, brain, and abdomen heightens the risk of hypoxemia. Consequently, it is imperative for VA-ECMO operators to determine the appropriate levels of ECMO and Impella support to adequately meet the oxygen demands of vital organs while alleviating pressure on the left ventricle.

Pulsatile circulation is essential for optimal cardiac function [31]. However, ECMO administration leads to non-pulsatile blood flow, potentially inducing adverse effects on both the heart and aorta. Our study revealed that hemodynamic pulsatility was most pronounced with ECMO combined with IABP, whereas it was significantly attenuated with ECMO combined with Impella.

Analysis of blood flow vector diagrams demonstrated significant alterations in the hemodynamics compared to ECMO treatment alone when combining ECMO with either IABP or Impella. The synergistic effect of these devices led to a more intricate hemodynamic profile compared to ECMO alone. The interaction between retrograde blood flow from the ECMO circuit and that originating from the failing heart resulted in modifications to the distribution of aortic perfusion [33]. This combined therapeutic approach influenced the location and characteristics of high-velocity regions and eddy currents, thereby generating complex perfusion patterns that could potentially precipitate clinical complications. Adjustment of Impella speed could profoundly impact patient hemodynamics, suggesting that modifications to auxiliary devices can alter hemodynamic parameters. Simulation outcomes indicated superior hemodynamic compatibility with ECMO combined with IABP relative to ECMO combined with Impella, showcasing certain advantages.

Wall shear stress (WSS) stands as a pivotal hemodynamic parameter, recognized for its significant role in vascular remodeling. Atherosclerosis correlates closely with WSS, with an optimal level typically falling within the range of 1.5-2.0 Pa [7]. Low WSS regions are predisposed to vasculopathy, while high WSS zones elevate the risk of hematological trauma. Notably, ECMO combined with Impella at lower flow rates promotes reduced WSS, mitigating the potential risk of hematological trauma. Our experimental findings underscore a

notable alteration in WSS with ECMO both with and without Impella support, whereas the impact of ECMO combined with IABP on WSS appeared relatively minor.

The duration of continuous ECMO support emerges as a crucial determinant of its vascular consequences [17]. Typically, the duration of circulatory assistance provided by Impella and IABP spans one to two weeks. According to studies elucidating the vascular mechanobiology of endothelial cells [1], this duration suffices to activate endothelial function, potentially leading to vascular dysfunction. Consequently, aberrant WSS distribution under Impella support may precipitate endothelial and vascular dysfunction. Considering hemodynamic principles, the distribution of WSS is governed by both the type and level of ECMO support. Hence, surgeons must judiciously select the appropriate unloading method and support level based on the patient's condition. Simultaneously, efforts should be directed towards minimizing the duration of unloading device support to mitigate the risk of endothelial and vascular dysfunction.

Limitations

This study still has certain limitations. It relies on an ideal geometric model with parameters obtained from existing literature. However, due to substantial inter-patient variability, this idealized geometric model may not adequately capture the diverse hemodynamic effects associated with the two VA-ECMO combinations. Future endeavors will involve the development of patient-specific models, incorporating boundary conditions derived from clinical practice to explore the nuances of VA-ECMO support types.

Furthermore, the CFD model employed in this study assumes a rigid aortic wall, whereas in reality, the aortic wall exhibits greater pliability. Addressing this would necessitate the implementation of more intricate fluid-structure interaction simulations, which are inherently more time-consuming. Undoubtedly, these potential enhancements will be duly considered in forthcoming studies.

Conclusions

Both the ECMO+Impella and ECMO+IABP combinations notably transformed the hemodynamics compared to ECMO treatment alone, introducing greater complexity. Thus, it

is imperative for ECMO operators to carefully select unloading modalities and determine the appropriate level of support for both ECMO and Impella. Further investigation into the impact of combined Impella and IABP use with ECMO on the aortic region will provide valuable insights for clinicians, enabling them to mitigate risks and optimize the management of patients undergoing ECMO support.

Acknowledgments

This work was supported by the National Key Research and Development Program of China (Grant No. 2022YFC2402600), Anhui Province Major Industrial Innovation Plan (Grant No. AHZDCYCX-YQ2023-04), Anhui Province Key Research and Development Plan (Grant No. 2023s07020011).

References

1. ANDO, J.,YAMAMOTO, K., *Vascular mechanobiology: endothelial cell responses to fluid shear stress.* Circ J, 2009. **73**(11): p. 1983-1992.
2. ATHANASIOU, L.S., NEZAMI, F.R.,EDELMAN, E.R., *Hemodynamic consequences of a multilayer flow modulator in aortic dissection.* Med Biol Eng Comput, 2019. **57**(9): p. 1861-1874.
3. AU, S.Y., FONG, K.M., TSANG, C.S., CHAN, K.A., WONG, C.Y., NG, W.G.,LEE, K.Y.M., *Veno-arterial extracorporeal membrane oxygenation with concomitant Impella versus concomitant intra-aortic-balloon-pump for cardiogenic shock.* Perfusion, 2023. **38**(1): p. 51-57.
4. BERGER, S.A.,JOU, L.D.J.A.R.O.F.M., *Flows in Stenotic Vessels.* 2000. **32**: p. 347-382.
5. BERNHARDT, A.M., HILLEBRAND, M., YILDIRIM, Y., HAKMI, S., WAGNER, F.M., BLANKENBERG, S., REICHENSPURNER, H.,LUBOS, E., *Percutaneous left atrial unloading to prevent pulmonary oedema and to facilitate ventricular recovery under extracorporeal membrane oxygenation therapy.* Interact Cardiovasc Thorac Surg, 2018. **26**(1): p. 4-7.
6. CARUSO, M.V., GRAMIGNA, V.,FRAGOMENI, G., *A CFD investigation of intra-aortic balloon pump assist ratio effects on aortic hemodynamics.* Biocybernetics and Biomedical Engineering, 2019. **39**(1): p. 224-233.
7. CARUSO, M.V., GRAMIGNA, V., RENZULLI, A.,FRAGOMENI, G., *Computational analysis of aortic hemodynamics during total and partial extracorporeal membrane oxygenation and intra-aortic balloon pump support.* Acta Bioeng Biomech, 2016. **18**(3): p. 3-9.
8. CENTOFANTI, P., ATTISANI, M., LA TORRE, M., RICCI, D., BOFFINI, M., BARONETTO, A., SIMONATO, E., CLERICI, A.,RINALDI, M., *Left Ventricular Unloading during Peripheral Extracorporeal Membrane Oxygenator Support: A Bridge To Life In Profound Cardiogenic Shock.* J Extra Corpor Technol, 2017. **49**(3): p. 201-205.
9. CHAR, S., FRIED, J., MELEHY, A., MEHTA, S., NING, Y., KURLANSKY, P.,TAKEDA, K., *Clinical efficacy of direct or indirect left ventricular unloading during venoarterial extracorporeal membrane*

oxygenation for primary cardiogenic shock. J Thorac Cardiovasc Surg, 2023. **165**(2): p. 699-707.e695.

10. DI MOLFETTA, A., ADACHI, I., FERRARI, G., GAGLIARDI, M.G., PERRI, G., IACOBELLI, R., QURESHI, A.M., DI PASQUALE, L., VERA, R.Z., GUCCIONE, P., DI MOLFETTA, M., CHIARIELLO, G.A., FILIPPELLI, S.,AMODEO, A., *Left ventricular unloading during extracorporeal membrane oxygenation - Impella versus atrial septal defect: A simulation study.* Int J Artif Organs, 2020. **43**(10): p. 663-670.
11. DONKER, D.W., BRODIE, D., HENRIQUES, J.P.S.,BROOMé, M., *Left Ventricular Unloading During Veno-Arterial ECMO: A Simulation Study.* Asaio j, 2019. **65**(1): p. 11-20.
12. ECKMAN, P.M., KATZ, J.N., EL BANAYOSY, A., BOHULA, E.A., SUN, B.,VAN DIEPEN, S., *Veno-Arterial Extracorporeal Membrane Oxygenation for Cardiogenic Shock: An Introduction for the Busy Clinician.* Circulation, 2019. **140**(24): p. 2019-2037.
13. GANDHI, K.D., MORAS, E.C., NIROULA, S., LOPEZ, P.D., AGGARWAL, D., BHATIA, K., BALBOUL, Y., DAIBES, J., CORREA, A., DOMINGUEZ, A.C., BIRATI, E.Y., BARAN, D.A., SERRAO, G., MAHMOOD, K., VALLABHAJOSYULA, S.,FOX, A., *Left Ventricular Unloading With Impella Versus IABP in Patients With VA-ECMO: A Systematic Review and Meta-Analysis.* Am J Cardiol, 2023. **208**: p. 53-59.
14. GAO, B., GU, K., ZENG, Y., LIU, Y.,CHANG, Y., *A blood assist index control by intraaorta pump: a control strategy for ventricular recovery.* Asaio j, 2011. **57**(5): p. 358-362.
15. GRANDIN, E.W., NUNEZ, J.I., WILLAR, B., KENNEDY, K., RYCUS, P., TONNA, J.E., KAPUR, N.K., SHAEFI, S.,GARAN, A.R., *Mechanical Left Ventricular Unloading in Patients Undergoing Venoarterial Extracorporeal Membrane Oxygenation.* J Am Coll Cardiol, 2022. **79**(13): p. 1239-1250.
16. GU, K., CHANG, Y., GAO, B., LIU, Y., ZHANG, Z.,WAN, F., *Lumped parameter model for heart failure with novel regulating mechanisms of peripheral resistance and vascular compliance.* Asaio j, 2012. **58**(3): p. 223-231.
17. GU, K., ZHANG, Y., GAO, B., CHANG, Y.,ZENG, Y., *Hemodynamic Differences Between Central ECMO and Peripheral ECMO: A Primary CFD Study.* Med Sci Monit, 2016. **22**: p. 717-726.
18. GU, K.Y., GAO, B., CHANG, Y.,LIU, Y.J., *Research on lumped parameter model based on intra-aorta pump.* Yiyong Shengwu Lixue/Journal of Medical Biomechanics, 2011. **26**: p. 367-372.
19. KIM, H.J., VIGNON-CLEMENTEL, I.E., FIGUEROA, C.A., JANSEN, K.E.,TAYLOR, C.A., *Developing computational methods for three-dimensional finite element simulations of coronary blood flow.* Finite Elements in Analysis and Design, 2010. **46**(6): p. 514-525.
20. LORUSSO, R., *Are two crutches better than one? The ongoing dilemma on the effects and need for left ventricular unloading during veno-arterial extracorporeal membrane oxygenation.* Eur J Heart Fail, 2017. **19**(3): p. 413-415.
21. MEANI, P., GELSOMINO, S., NATOUR, E., JOHNSON, D.M., ROCCA, H.B., PAPPALARDO, F., BIDAR, E., MAKHOUL, M., RAFFA, G., HEUTS, S., LOZEKOOT, P., KATS, S., SLUIJPERS, N., SCHREURS, R., DELNOIJ, T., MONTALTI, A., SELS, J.W., VAN DE POLL, M., ROEKAERTS, P., POELS, T., KORVER, E., BABAR, Z., MAESSEN, J.,LORUSSO, R., *Modalities and Effects of Left Ventricle Unloading on Extracorporeal Life support: a Review of the Current Literature.* Eur J Heart Fail, 2017. **19 Suppl 2**: p. 84-91.
22. MEANI, P.,PAPPALARDO, F., *The step forward for VA ECMO: left ventricular unloading!* J Thorac Dis, 2017. **9**(11): p. 4149-4151.

23. MOAZZAMI, K., DOLMATOVA, E.V., COCKE, T.P., ELMANN, E., VAIDYA, P., NG, A.F., SATYA, K.,NARAYAN, R.L., *Left Ventricular Mechanical Support with the Impella during Extracorporeal Membrane Oxygenation.* J Tehran Heart Cent, 2017. **12**(1): p. 11-14.
24. NEIDLIN, M., CORSINI, C., SONNTAG, S.J., SCHULTE-EISTRUP, S., SCHMITZ-RODE, T., STEINSEIFER, U., PENNATI, G.,KAUFMANN, T.A.S., *Hemodynamic analysis of outflow grafting positions of a ventricular assist device using closed-loop multiscale CFD simulations: Preliminary results.* J Biomech, 2016. **49**(13): p. 2718-2725.
25. NEZAMI, F.R., KHODAEE, F., EDELMAN, E.R.,KELLER, S.P., *A Computational Fluid Dynamics Study of the Extracorporeal Membrane Oxygenation-Failing Heart Circulation.* Asaio j, 2021. **67**(3): p. 276-283.
26. PAPPALARDO, F., SCHULTE, C., PIERI, M., SCHRAGE, B., CONTRI, R., SOEFFKER, G., GRECO, T., LEMBO, R., MüLLERLEILE, K., COLOMBO, A., SYDOW, K., DE BONIS, M., WAGNER, F., REICHENSPURNER, H., BLANKENBERG, S., ZANGRILLO, A.,WESTERMANN, D., *Concomitant implantation of Impella(®) on top of veno-arterial extracorporeal membrane oxygenation may improve survival of patients with cardiogenic shock.* Eur J Heart Fail, 2017. **19**(3): p. 404-412.
27. PEDLEY, T.J., *The Fluid Mechanics of Large Blood Vessels*. Cambridge Monographs on Mechanics. 1980, Cambridge: Cambridge University Press.
28. RIKHTEGAR NEZAMI, F., ATHANASIOU, L.S., AMRUTE, J.M.,EDELMAN, E.R., *Multilayer flow modulator enhances vital organ perfusion in patients with type B aortic dissection.* Am J Physiol Heart Circ Physiol, 2018. **315**(5): p. H1182-h1193.
29. ROBERTS, N., CHANDRASEKARAN, U., DAS, S., QI, Z.,CORBETT, S., *Hemolysis associated with Impella heart pump positioning: In vitro hemolysis testing and computational fluid dynamics modeling*. Int J Artif Organs, 2020: p. 391398820909843.
30. RUSSO, J.J., ALEKSOVA, N., PITCHER, I., COUTURE, E., PARLOW, S., FARAZ, M., VISINTINI, S., SIMARD, T., DI SANTO, P., MATHEW, R., SO, D.Y., TAKEDA, K., GARAN, A.R., KARMPALIOTIS, D., TAKAYAMA, H., KIRTANE, A.J.,HIBBERT, B., *Left Ventricular Unloading During Extracorporeal Membrane Oxygenation in Patients With Cardiogenic Shock.* J Am Coll Cardiol, 2019. **73**(6): p. 654-662.
31. SAITO, S., NISHINAKA, T.,WESTABY, S., *Hemodynamics of chronic nonpulsatile flow: implications for LVAD development.* Surg Clin North Am, 2004. **84**(1): p. 61-74.
32. SCHMACK, B., SEPPELT, P., WEYMANN, A., ALT, C., FARAG, M., ARIF, R., DOESCH, A.O., RAAKE, P.W., KALLENBACH, K., MANSUR, A., POPOV, A.F., KARCK, M.,RUHPARWAR, A., *Extracorporeal life support with left ventricular decompression-improved survival in severe cardiogenic shock: results from a retrospective study.* PeerJ, 2017. **5**: p. e3813.
33. STEVENS, M.C., CALLAGHAN, F.M., FORREST, P., BANNON, P.G.,GRIEVE, S.M., *Flow mixing during peripheral veno-arterial extra corporeal membrane oxygenation - A simulation study.* J Biomech, 2017. **55**: p. 64-70.
34. WANG, Y., WANG, J., PENG, J., HUO, M., YANG, Z., GIRIDHARAN, G.A., LUAN, Y.,QIN, K., *Effects of a Short-Term Left Ventricular Assist Device on Hemodynamics in a Heart Failure Patient-Specific Aorta Model: A CFD Study.* Front Physiol, 2021. **12**: p. 733464.
35. XIAO, N., ALASTRUEY, J.,ALBERTO FIGUEROA, C., *A systematic comparison between 1-D and 3-D hemodynamics in compliant arterial models.* Int J Numer Method Biomed Eng, 2014. **30**(2): p. 204-231.